Optoelectronic property refinement of FASnI(3) films for photovoltaic application

Jorim Okoth Obila, Hongwei Lei, Elijah Omollo Ayieta, Alex Awuor Ogacho, Bernard O. Aduda and Feng Wang

Obila, J. O., Lei, H., Ayieta, E. O., Ogacho, A. A., Aduda, B. O., Wang, F., (2021), Optoelectronic property refinement of FASnI(3) films for photovoltaic application, *Materials letters (General ed.)*, 300, 130099. https://doi.org/10.1016/j.matlet.2021.130099

Original publication available at:
https://doi.org/10.1016/j.matlet.2021.130099

Optoelectronic Property Refinement of $FASnI_3$ films for Photovoltaic Application

Jorim Okoth Obila[a], Hongwei Lei[b,c], Elijah Omollo Ayieta[a], Alex Awuor Ogacho[a], Bernard O. Aduda[a], Feng Wang[b]

[a] Department of Physics, University of Nairobi, Nairobi, Kenya.

[b] Department of Physics, Chemistry and Biology (IFM), Linköping University, Linköping, Sweden.

[c] College of Science, Huazhong Agricultural University, Wuhan, China.

Abstract

Tin (Sn) is a promising substitute for lead (Pb) in organic-inorganic hybrid halide perovskite-photovoltaic devices, but it is prone to delivering low power conversion efficiencies (PCEs) due to the poor quality of Sn-perovskite films. In this work, anilinium hypophosphite (AHP) co-additive is used to fabricate high-quality $FASnI_3$ (FA^+: formamidinium) perovskite films with a high charge carrier lifetime and improved morphology. AHP-based perovskite films based solar cells deliver a high power conversion efficiency (PCE) of up to 5.48 %.

Keywords

Sn-perovskite, phase-aggregation, anilinium hypophosphite.

Introduction

Tin-perovskites (SPVKs) have excellent optoelectrical properties such as small exciton binding energies, high charge carrier mobilities, and high-light absorption coefficient [1]. Solar cells based on SPVKs exhibit low efficiencies with the best photo conversion efficiency (PCE) standing at 13 %, and low reproducibility [2]. The low efficiency is limited by the ease of oxidation of Sn^{2+} to Sn^{4+} in SPVKs [3], which leads to Sn-vacancies charge recombination centers, leading to energy losses and low PCE [1].

Reducing agents [4], film morphology optimization [5], and device structure modification [6] have been used to address the low PCE and oxidation issues of Sn^{2+} in SPVK devices. A typical example is tin fluoride (SnF_2), which has been widely employed as an antioxidation agent in SPVK-films [7]. However, the aggregation of SnF2 leads to poor film morphology and acts as charge trap centers, hence lowers the PCE of devices [8].

In our previous study, we successfully used anilinium hypophosphite (AHP) as a co-additive in $FA_{0.5}MA_{0.45}PEA_{0.05}SnI_3$ perovskites to eliminate the phase separation by forming SnF_2-AHP complex [9]. Here, we further extend the study to $FASnI_3$-perovskite with a great

potential to achieve higher PCEs [10]. We demonstrate that AHP additive can greatly improve the $FASnI_3$ film quality with better optoelectronic properties including optimized morphologies, increased crystallinity, and prolonged carrier lifetime. Therefore, $FASnI_3$ solar cells generate enhanced photovoltaic performance.

Experimental Section

Materials: Poly (3,4-ethylene dioxythiophene) polystyrene sulfonate (PEDOT:PSS) is from Ossila. Formamidinium iodide (FAI) (>98%), tin (ii) iodide (SnI_2) (99.999%), (SnF_2) (>99%), [6,6]-phenyl-C60-butyric acid methyl ester ($PC_{60}BM$), Bathocuproine (BCP) (99.99%), *N,N*–dimethylformamide (DMF) (99.8%), and dimethyl sulfoxide (DMSO) (99.8%), anilinium hypophosphite (97%), and chlorobenzene (CB) (99.8%) are from Sigma Aldrich.

Solution Preparation: The solvent contained a mixture of DMF and DMSO in the ratio of 4:1. The reference and the AHP precursor solution contained $FAI:SnI_2:0.1SnF_2$ and $FAI:SnI_2:0.1SnF_2:0.05AHP$, respectively. 20.0 mg $PC_{60}BM$ and 0.5 mg BCP was dissolved in 1 ml CB, and 1 ml ethanol, respectively.

Device Fabrication: The devices were built on a pre-cleaned ITO-glass substrate. 30 µl PEDOT:PSS was spin-coated at 5000 rpm for 40 s, and dried at 150 ℃ for 30 minutes. 20 µl perovskite precursor solution was spin-coated at 5000 rpm for 40 s in two steps on the PEDOT substrate inside a glovebox, 150 µL CB was dripped on the substrate at the 22nd second of spinning, followed by annealing at 80 ℃ for 30 minutes. 20 µl $PC_{60}BM$ was spin-coated on the cooled perovskite substrate at 2000 rpm for 30 s and annealed at 100 ℃ for 10 minutes. 75 µl BCP solution was spin-coated on $PC_{60}BM$ at 5000 rpm for 40 s. 70 nm silver (Ag) was evaporated on the BCP layer to complete the devices.

Film and device characterizations: The films and devices were characterized as described in our previous paper [9].

Results and Discussion

We used solvent engineering to deposit films with improved substrate coverage. The SEM image of the reference film containing 10% SnF_2, shown in Fig. 1(a), showed white-rods-like phases on the film surface. From the inset image, under high magnification. The white phases, contributing to poor morphology, appear on the surface of the film. The white phases are attributed to segregation caused by the addition of SnF_2 [11], the additional phases act as charge trap centers [12]. The pristine films bear few pinholes which reduce the

performance of devices as they allow direct contact between the electron transport layer (ETL) and hole transport medium (HTM) leading to a reduced fill-factor (FF) due to poor charge transport [13]. We used AHP as a co-additive to eliminate the phase segregation and the pinholes, as shown in Fig. 1(b). SnF_2 can interact with AHP to form an AHP·SnF_2-complex, hence lead to the disappearance of the aggregates [9]. The complex passivates both the film surface and grain boundaries, this is evident from the complete disappearance of the pinholes and the clarity of the grain boundaries, as shown in Fig 1(b)-inset image. The reference films were not stable under the SEM electron beam, this resulted in poor image quality (the inset image in Fig. 1(a)), a sign of degradation. The grain sizes of the pristine and the AHP films ranged between 334 and 1161 nm with an average size of 720 nm while the grain sizes AHP films ranged between 507 and 1392 nm with an average size of 775 nm. SEM-EDS elemental mapping was conducted on the perovskite films to investigate the distribution of the additives on the film surfaces, as shown in Fig.1(c and d). The distribution of the characteristic elements of SnF_2 and AHP, F and P, was uniform, as shown in Fig.1(c and d), respectively. The F and P distribution is inhomogeneous on the surface of the film, which is a sign that most of the complex formed is heavily positioned along the grain boundaries, with only a few of them resting on the perovskite grains.

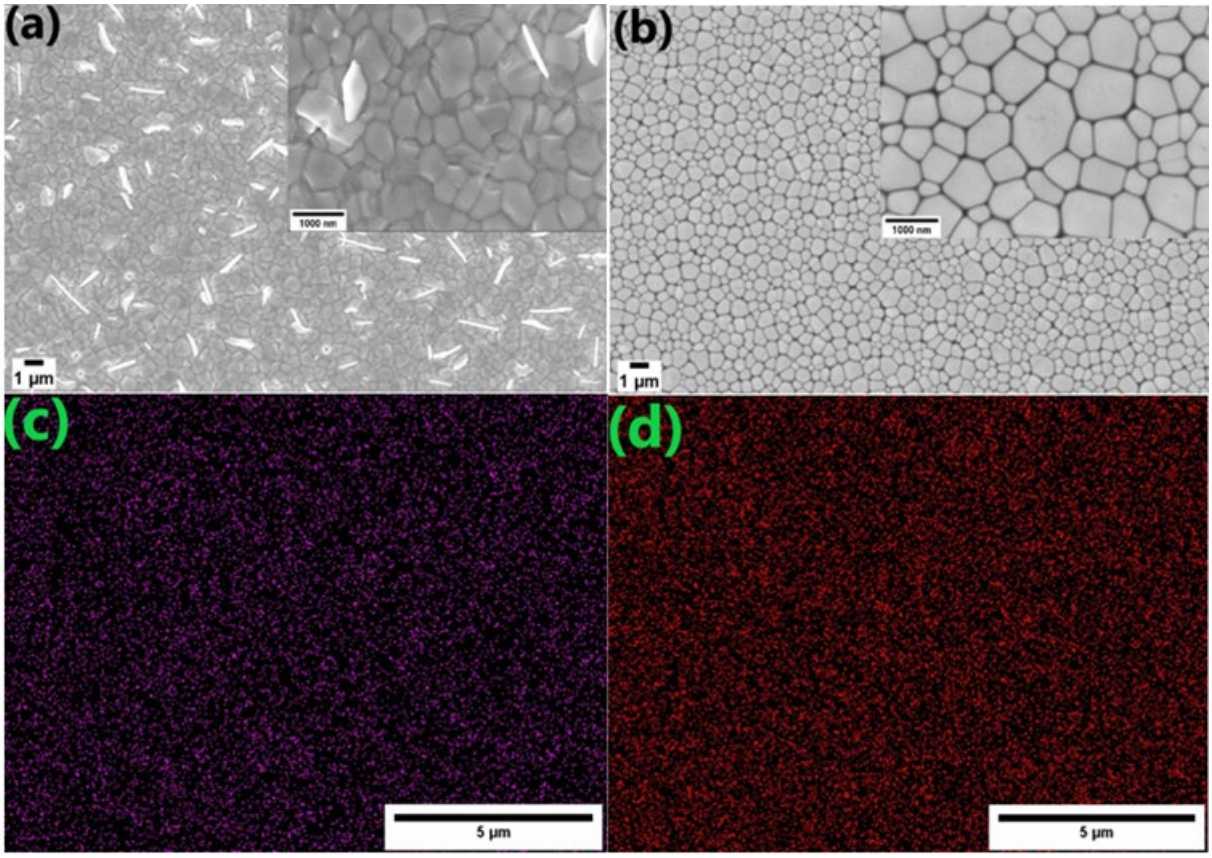

Fig. 1: Top-view of SEM images of (a) reference and, (b) AHP-based $FASnI_3$ films (the insets are highly magnified images for easy visibility of the images' features. (c) SEM-EDS elemental mapping of (c) F and (d) P distribution on the film surface.

The XRD main peaks of $FASnI_3$, as presented in Fig. 2(a), are located at 14.0°, 24.4°, 28.1°, 31.6°, 40.4°, 42.9°, which are assigned to (100), (102), (200), (122), (222), and (213) crystal planes of the orthorhombic ($Amm2$) structure, respectively. The diffraction peak intensity of $FASnI_3$ absorber film is pronounced when AHP co-additive was used, confirming improved crystallinity. The absorption spectra of films with and without AHP are shown in Fig. 2(b) and the inset is a graph of $(\alpha hv)^2$ versus (hv) to estimate the bandgaps of the films. The bandgap of the $FASnI_3$ films was of 1.39 eV. AHP addition into the film slightly increased the absorption of the film due to improved film qualities as seen from the SEM data. Photoluminescence (PL) measurement, was conducted to verify the optical properties and to understand the charge dynamics of the perovskite films (Fig. 2(c),). The PL intensity of AHP-based films is higher, indicating that a combination of the two additives can passivate defects in Sn-perovskite films, leading to better performing devices [14]. The time-resolved PL (TRPL) spectra, shown in Fig. 2(d), were fitted and the average carrier lifetime (τ_{avg})

calculated. The AHP based films showed increased carrier lifetime from 1.16 ns to 1.83 ns, which is an indication of reduced trap state densities in the films [15].

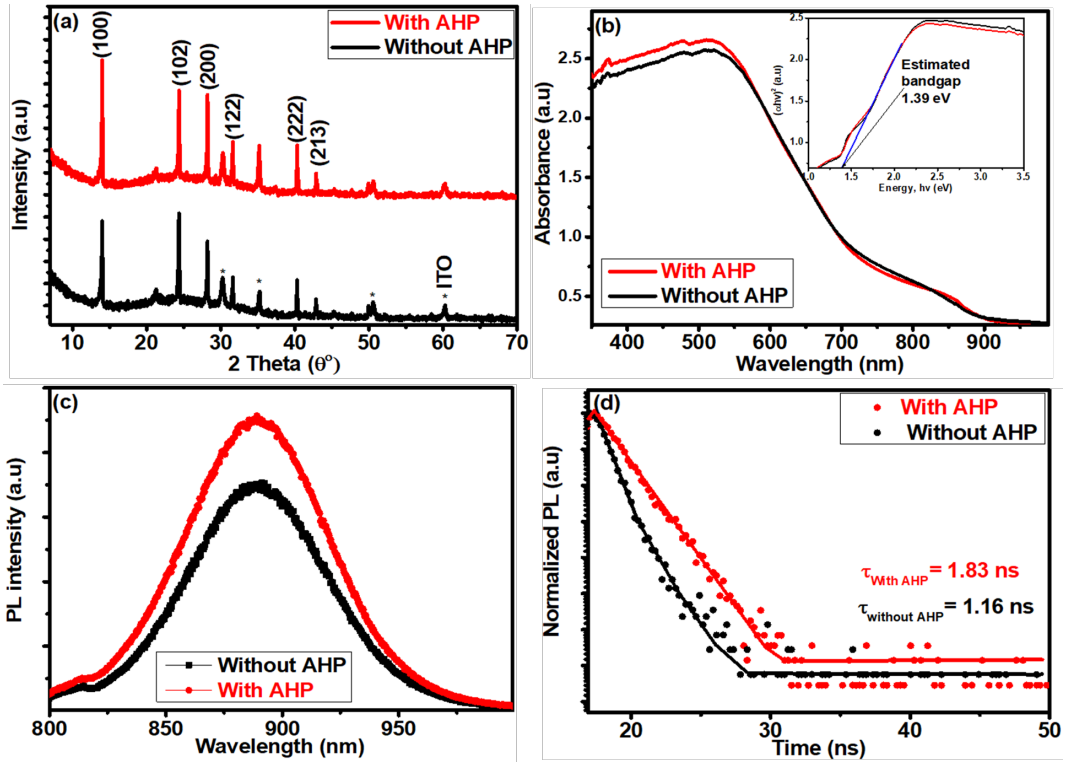

Fig. 2: (a) The XRD pattern, (b) the UV-visible absorption spectra, the inset figure is a plot of $(\alpha\,\mathrm{hv})^2$ versus (hv) used in bandgap estimation, (c) PL spectra, and (d) TRPL spectra of $FASnI_3$ films.

Table 1 summarizes the results of the photocurrent density-voltage (J-V) measurements of the devices (active-area: 0.0725 cm^{-2}). The V_{oc} and the FF of the devices were remarkably improved when AHP was incorporated in the absorber layer, leading to an enhancement of PCE from 4.04 % of the reference cell to 5.48 %. The reference devices showed obvious hysteresis as shown in Fig. 3(a) and the possible causes of hysteresis include unwanted phases, charge accumulation within the solar cell, and defects [16]. The addition of AHP improved the properties of $FASnI_3$ films which leads to less/no defects and enhanced charge transfer between the perovskite and the ETL, thus resulted in reduced/negligible hysteresis [12]. The AHP champion device exhibited a steady J_{sc} of 19.22 $mAcm^{-2}$ for 120 s at a bias of 0.29 V, as shown in Fig. 3(b). Figure 3(c) is a histogram showing the performance of the fabricated devices. The external quantum efficiency (EQE) of the champion devices was determined, Fig. 3(d), the EQE of AHP-based devices was slightly higher. The integrated J_{sc} values of the devices were different from the J_{sc} measured from the J-V curves, possibly

because the EQE of the cells were measured in air thereby exposing the devices to some degradation.

Table 1: The performance of the fabricated solar cells.

Sample	V_{OC} (V)		J_{SC} (mA cm^{-2})		FF (%)		PCE (%)	
	Forward	Backward	Forward	Backward	Forward	Backward	Forward	Backward
Without AHP (Champion)	0.33	0.30	-21.00	-18.40	57.93	40.61	4.04	2.26
Without AHP (Average)	0.32±0.01	0.31±0.01	-21.91±2.79	-21.68±2.95	53.18±4.89	46.19±3.52	3.81±0.17	3.06±0.58
With AHP (Champion)	0.37	0.37	-22.25	-22.0805	66.35702	64.90787	5.48253	5.23669
With AHP (Average)	0.34±0.02	0.33±0.02	-22.80±2.45	-22.79±2.67	57.79±5.06	54.13±6.41	4.43±0.41	4.02±0.61

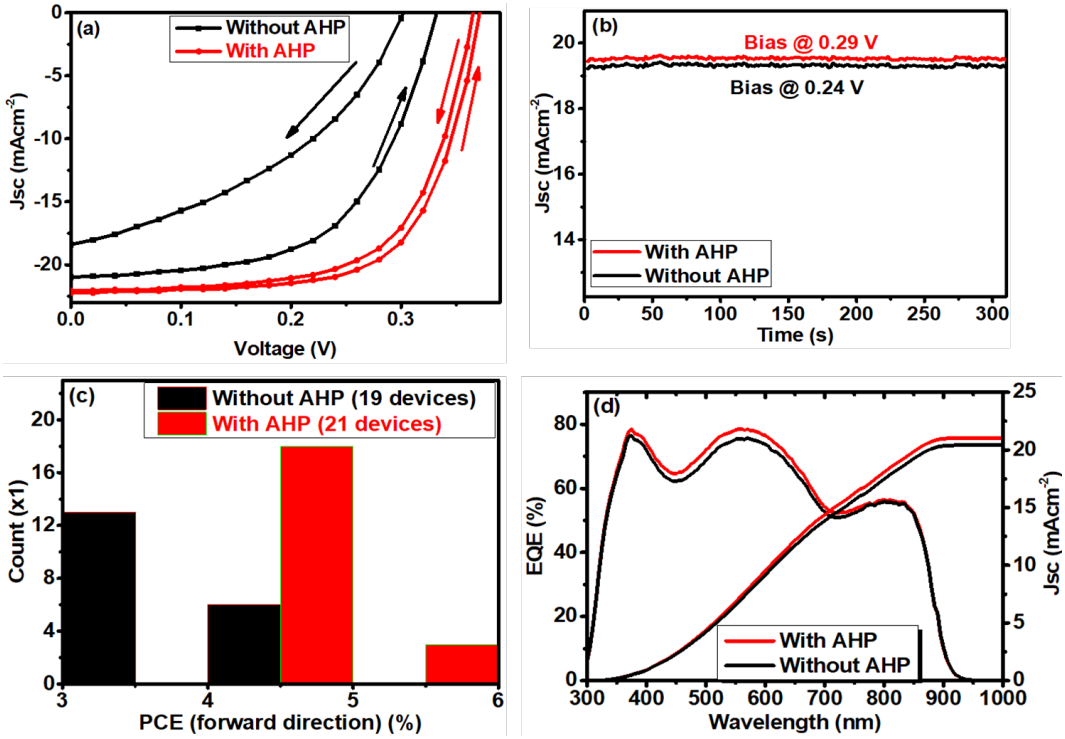

Fig. 3: (a) The current density-voltage (J-V) curves of champion devices, (b) the steady-state current of the champion devices, (c) the histogram of the PCEs of the fabricated devices, and (d) the EQE curves of the champion devices.

Conclusion

The performance of perovskite devices is heavily based on the quality of the absorber material. We showed that a combination of anilinium hypophosphite and SnF_2 additives can improve $FASnI_3$-perovskite films quality and optoelectronic properties including optimized morphologies, increased crystallinity, and prolonged carrier lifetime and consequently lead to solar cells with enhanced performance.

Acknowledgment

We thank the International Science Programme in Physics (Sweden), PASET regional scholarship and innovation fund, National Natural Science Foundation of China (Grant No. 11904115), the Swedish Research Council (VR starting grant: 2018-04809), and the Swedish STINT grant (CH2018-7655) for financial support. We thank Prof. Feng Gao for the laboratory and chemicals.

Conflict of Interest

The authors declare no conflict of interest.

References

[1] C.H. Ng, K. Hamada, G. Kapil, M.A. Kamarudin, Z. Wang, S. Likubo, Q. Shen, K. Yoshino, T. Minemoto, S. Hayase, J. Mater. Chem. A. 8 (2020) 2962–2968.

[2] T. Nakamura, S. Yakumaru, M.A. Truong, K. Kim, J. Liu, S. Hu, K. Otsuka, R. Hashimoto, R. Murdey, T. Sasamori, H. Do Kim, H. Ohkita, T. Handa, Y. Kanemitsu, A. Wakamiya, Nat. Commun. 11 (2020) 3008.

[3] Y. Yan, T. Pullerits, K. Zheng, K. Zheng, Z. Liang, ACS Energy Lett. 5 (2020) 2052–2086.

[4] U. Krishnan, J. Photonics Energy. 9 (2019) 1.

[5] F. Igbari, Z.K. Wang, L.S. Liao, Adv. Energy Mater. 9 (2019) 1–32.

[6] W.F. Yang, F. Igbari, Y.H. Lou, Z.K. Wang, L.S. Liao, Adv. Energy Mater. 10 (2020).

[7] M. Konstantakou, T. Stergiopoulos, J. Mater. Chem. A. 5 (2017) 11518–11549.

[8] X. Jiang, F. Wang, Q. Wei, H. Li, Y. Shang, W. Zhou, C. Wang, P. Cheng, Q. Chen, L. Chen, Z. Ning, Nat. Commun. 11 (2020) 1–7.

[9] J.O. Obila, H. Lei, E.O. Ayieta, A.A. Ogacho, B.O. Aduda, W. Feng, New J. Chem. (2021).

[10] W. Ke, C.C. Stoumpos, M.G. Kanatzidis, Adv. Mater. 31 (2019).

[11] S. Shao, J. Liu, G. Portale, H.H. Fang, G.R. Blake, G.H. ten Brink, L.J.A. Koster, M.A. Loi, Adv. Energy Mater. 8 (2018).

[12] J. Chen, N.G. Park, Adv. Mater. 31 (2019) 1–56.

[13] H. Yao, F. Zhou, Z. Li, Z. Ci, L. Ding, Z. Jin, Adv. Sci. 7 (2020).

[14] Z. Lin, C. Liu, G. Liu, J. Yang, X. Duan, L. Tan, Y. Chen, Chem. Commun. 56 (2020)

4007–4010.

[15] E. Jokar, P.Y. Cheng, C.Y. Lin, S. Narra, S. Shahbazi, E.W.G. Diau, ACS Energy Lett. 6 (2021) 485–492.

[16] L.K. Ono, S.R. Raga, M. Remeika, A.J. Winchester, A. Gabe, Y. Qi, J. Mater. Chem. A. 3 (2015) 15451–15456.